Astronomy & Astrophysics manuscript no. densegas˙vs˙Z
December 8, 2016
© ESO 2016

arXiv:1612.02196v1 [astro-ph.GA] 7 Dec 2016

Dense gas in low-metallicity galaxies

J. Braine[1], Y. Shimajiri[2], P. André[2], S. Bontemps[1], Yu Gao[3,4], Hao Chen[5,6,7], and C. Kramer[8]

[1] Laboratoire d'Astrophysique de Bordeaux, Univ. Bordeaux, CNRS, B18N, alle Geoffroy Saint-Hilaire, 33615 Pessac, France.
e-mail: jonathan.braine@u-bordeaux.fr
[2] Laboratoire AIM, CEA/DRF–CNRS–Université Paris Diderot, IRFU/Service dAstrophysique, C.E. Saclay, Orme des Merisiers, 91191 Gif-sur-Yvette, France
[3] Purple Mountain Observatory, Chinese Academy of Sciences, 2 West Beijing Road, Nanjing 210008, P. R. China;
[4] Key Laboratory of Radio Astronomy, Chinese Academy of Sciences, Nanjing 210008, P. R. China
[5] School of Astronomy and Space Science, Nanjing University, Nanjing 210093, P. R. China
[6] Key Laboratory of Modern Astronomy and Astrophysics, Nanjing University, Nanjing 210093, P. R. China
[7] Collaborative Innovation Center of Modern Astronomy and Space Exploration, Nanjing 210093, P. R. China
[8] Instituto Radioastronoma Milimétrica, Av. Divina Pastora 7, Nucleo Central, 18012 Granada, Spain

Received xxxx; accepted xxxx

ABSTRACT

Stars form out of the densest parts of molecular clouds. Far-IR emission can be used to estimate the Star Formation Rate (SFR) and high dipole moment molecules, typically HCN, trace the dense gas. A strong correlation exists between HCN and Far-IR emission, with the ratio being nearly constant, over a large range of physical scales. A few recent observations have found HCN to be weak with respect to the Far-IR and CO in subsolar metallicity (low-Z) objects. We present observations of the Local Group galaxies M 33, IC 10, and NGC 6822 with the IRAM 30meter and NRO 45m telescopes, greatly improving the sample of low-Z galaxies observed. HCN, HCO^+, CS, C_2H, and HNC have been detected. Compared to solar metallicity galaxies, the Nitrogen-bearing species are weak (HCN, HNC) or not detected (CN, HNCO, N_2H^+) relative to Far-IR or CO emission. HCO^+ and C_2H emission is normal with respect to CO and Far-IR. While ^{13}CO is the usual factor 10 weaker than ^{12}CO, $C^{18}O$ emission was not detected down to very low levels. Including earlier data, we find that the HCN/HCO^+ ratio varies with metallicity (O/H) and attribute this to the sharply decreasing Nitrogen abundance. The dense gas fraction, traced by the HCN/CO and HCO^+/CO ratios, follows the SFR but in the low-Z objects the HCO^+ is much easier to measure. Combined with larger and smaller scale measurements, the HCO^+ line appears to be an excellent tracer of dense gas and varies linearly with the SFR for both low and high metallicities.

Key words. Galaxies: Individual: M 33 – Galaxies: Individual: IC 10 – Galaxies: Individual: NGC 6822 – Galaxies: Local Group – Galaxies: ISM – Stars: Formation

1. Introduction

Stars are believed to condense out of prestellar cores within the densest parts, clumps and/or filaments above $A_v \sim 8$ or $n_{H2} \sim 1 - 2 \times 10^4$ cm^{-3} (André et al. 2010; Lada et al. 2010) of giant molecular clouds (GMCs). To study the link between gas and star formation, it is important to observe molecules which emit preferentially in these environments. HCN and HCO^+ are used to trace dense molecular gas because their dipole moments are high, such that they are thermalized by collisions only at high densities ($n(H_2) > 10^4 cm^{-3}$) even for the lowest transitions. If star formation proceeds in a quasi-universal manner in all dense clumps/filaments (André et al. 2014), then we expect the star formation rate (SFR) to be strongly and linearly correlated with the dense gas mass. In terms of observables, we expect the Far-InfraRed (FIR) emission to follow that of HCN and HCO^+. A large number of articles (e.g. Gao & Solomon 2004a,b; Wu et al. 2005; Gao et al. 2007; Baan et al. 2008; Graciá-Carpio et al. 2008; Wu et al. 2010; García-Burillo et al. 2012; Liu & Gao 2010; Lada et al. 2012; Kepley et al. 2014) have studied the link between HCN, and HCO^+ in more recent work, with far-infrared (FIR) luminosities in a variety of environments. They tend to show that FIR and HCN emission (and often HCO^+) are closely linked. Recent work by Chen et al. (2015) and Usero et al. (2015) showed that HCN emission, both with respect to the total molecular gas mass (as traced by CO) and to the SFR (as traced by Far-IR emission), was significantly stronger in galactic nuclei as compared to galactic disks.

Both HCN and HCO^+ have low abundances, orders of magnitude lower than CO, so their abundances can be significantly modified by changes in the chemical network leading to their formation (e.g. López-Sepulcre et al. 2010), and these changes are not necessarily be linked to star formation. Unlike HCN, HCO^+ is a molecular ion and affected by the ionization equilibrium. In addition, the collisional cross-section of HCO^+ is much larger than that of HCN. Both molecules are linear and thus are described by a single rotational quantum number. Elemental abundance ratios are not always constant and can affect the production of molecules.

In particular, the Nitrogen abundance tends to decrease more quickly than the Oxygen or Carbon in low-metallicity galaxies. In galactic disks, the HCN/CO and HCO^+/CO line intensity ratios (1–0 transition, expressed in Kkm/s) are about 2%, although in galactic nuclei and starburst galaxies these ratios tend to be higher (see references in first paragraph and Brouillet et al. (2005) for M 31 and Kuno et al. (1995) for M 51). Recently, Buchbender et al. (2013) showed that in the roughly half-solar metallicity galaxy M 33, the emission from the dense gas tracers HCN and HCO^+ was weak relative to CO, particularly HCN. Gratier et al. (2010a) actually failed to detect HCN in the CO-

bright region Hubble V in the Local Group low-metallicity galaxy NGC 6822, with a 1σ limit 180 times weaker than the CO. The variations between HCO^+ and HCN show that new observing programs require both tracers as HCO^+ is probably less affected by metallicity variations and tends to be stronger than HCN in disks but not in nuclei.

Descending the mass/morphology/metallicity sequence from M 31 to M 33 to the Magellanic Clouds (MC), the HCO^+/HCN ratio increases from 1.2 in M 31 (Brouillet et al. 2005, particularly figure 3), 1.5 (range from 1.1 to 2.5) in M 33 (Buchbender et al. 2013), to $\sim$ 1.8 in the Large MC (Chin et al. 1997) and 3 in the Small MC (Chin et al. 1998, single position). Within M 31, a rather rough trend can be seen with radius, with the HCO^+/HCN ratio increasing from 1 in the inner parts to $\sim$ 1.4 in the outer disk. Are these variations in the HCN/CO ratio and the HCO^+/HCN ratio due to metallicity?

Recent comparisons between Galactic and extragalactic studies of the SF rate (Heiderman et al. 2010; Lada et al. 2012) suggest that there may a quasi-universal "star formation law" such that dense gas ($\geq 10^4$ cm^{-3}) is converted into stars at a constant rate with a constant stellar initial mass function (IMF). It has been proposed that this may be the result of the quasi-universal filamentary structure of molecular clouds (André et al. 2014).

In this work, our goal is to understand how to use dense gas tracers in low-metallicity galaxies. More precisely, we wish to measure the variation with metallicity of the link between the dense gas tracers HCN and HCO^+ and the FIR and CO emission. In order to keep observing times reasonable, only positions/objects with CO lines brighter than ~0.5K (T_{mb} at $\sim$ 20" resolution) were observed. In order that the linear resolution be comparable to the size of a molecular cloud or cloud complex ($\sim$ 100pc), we restricted our observations to Local Group galaxies which cover a rather complete range in metallicity. Most extragalactic studies focus on the central regions – whether by choice or simply due to the single pointing per object – where it is known that gas is on average denser. By observing Local Group objects, we observe identifiable positions in disks where a wealth of other data is available, such as HI column densities and several tracers of the SFR (Hα, FIR, FUV...). Detailed analyses of the biases and validity of a broad variety of SFR tracers can be found in Boquien et al. (2011) and Galametz et al. (2013).

While the major starbursts (ULIRGs) observed in Gao & Solomon (e.g. 2004b,a) likely have a solar metallicity, this is not the general case for distant galaxies. Only by studying the role of metallicity in local galaxies can we evaluate the "universality" of the "dense gas – star formation" relation and its tentative application to high-redshift galaxies.

In addition to HCN(1–0) and HCO^+(1–0), the HNC(1–0), N_2H^+(1–0), CS(2–1), and CCH lines were observed and, with the exception of N_2H^+, detected. The HCN/HNC ratio is typically about 3 in the Magellanic clouds (Chin et al. 1997) but closer to unity in e.g. IC342 (Meier & Turner 2005). Galactic observations suggest that the HCN/HNC ratio can be used as a probe of physical conditions (HCN and HNC dipole moments are virtually identical). The HCN/HNC ratio is typically greater than unity, sometimes much greater, in warm GMC cores (e.g. Hirota et al. 1998) but can be as low as 0.1 or 0.2 in dark cloud cores (e.g. Tennekes et al. 2006, and references therein). Thus, detected variations in this ratio are likely a sensitive temperature indicator. The N_2H^+ line is a classical tracer of cool and dense regions in the Galaxy as it depletes only very weakly onto dust grains. With 2 Nitrogen atoms, N_2H^+ should be strongly affected by metallicity variations, providing a check for the HCN/HCO^+ ratio as a function of metallicity.

Source	distance (kpc)	metallicity (Z_{sol})	RA (J2000)	Dec (J2000)
M 33a	840	0.5	01:34:34.5	30:46:30
M 33b	840	0.5	01:34:33.56	30:46:46
M 33c	840	0.5	01:34:32.3	30:46:58
IC10b8	950	0.35	0:20:21.6	59:17:09
IC10b9	950	0.35	0:20:22.9	59:21:18
IC10b11	950	0.35	0:20:27.7	59:17
N6822HubV	490	0.3	19:44:52.80	-14:43:11

Table 1. Sources and positions observed in M 33, IC 10, and NGC 6822. Distances are from Galleti et al. (2004) for M 33, Hunter (2001) for IC 10, Mateo (1998) for NGC 6822. Metallicities are from Magrini et al. (2009) for M 33, Magrini & Gonçalves (2009) for IC10, Skillman et al. (1989) for NGC 6822. Positions are chosen from our data (Gratier et al. 2010b; Druard et al. 2014; Gratier et al. 2010a) for M 33 and NGC 6822 and Leroy et al. (2006) for IC 10.

We have selected 3 positions in M 33 in/near the giant HII region NGC 604, clouds B8 B9 and B11 identified by Leroy et al. (2006) in IC10, and Hubble V in NGC6822 in which HCN was not detected (and HCO^+ not observed by Gratier et al. (2010a). Figures 1, 2, and 3 show the positions and beamsizes of the observations on respectively IC 10, NGC 6822, and M 33 as seen at 24μm with Spitzer. For M 33, the positions observed in HCN/HCO^+ by Buchbender et al. (2013) are also shown. We choose to show the 24μm emission because it is a high angular resolution tracer of star formation (e.g. Calzetti et al. 2010). Table 1 gives the sources, assumed distances, metallicities and positions of the new observations.

2. Observations and data reduction

2.1. IRAM 30meter observations

The IRAM 30meter telescope [1] was used in Nov/Dec 2014 and May 2015 to observe 3 positions in IC 10, the Hubble V HII region in NGC 6822, and a position in M 33 (M 33a). The coordinates are given in Table 1. The E090 and E230 dual polarization sideband-separating EMIR receivers (Carter et al. 2012) were used to observe the lines listed in Table 2. The very broad FTS backends were used, providing 195kHz resolution (channel separation) over up to 16GHz. The data were taken using the wobbler, with a throw of typically 2 arcminutes, making sure not to risk having emission in the reference position. Telescope focus was checked at the beginning of each day and pointing was checked every 1.5 – 2 hours. A line source, generally DR21 which is well-known to our group, was observed each day to check the tuning. The beamsize is about 28″ at 90GHz, 22″ for ^{13}CO(1–0) and 11″ at the frequencies we have used in the 1mm band.

System temperatures varied from 75–120 K for the lines near 90GHz to 100-160 K at 110GHz and 200 K at 115GHz and ~300 K in the 1mm band. Spectra were individually inspected and a small number of spectra identified as being of poor quality were dropped. The spectra for each line and source were then averaged and a continuum level (i.e. a zero-order baseline) subtracted if necessary. All spectra are presented on the main beam

[1] Based on observations carried out with the IRAM 30m Telescope. IRAM is supported by INSU/CNRS (France), MPG (Germany) and IGN (Spain)

Line	Frequency (GHz)
HCN($J = 1 - 0$)	88.6318475
HCO^+($J = 1 - 0$)	89.18853
HNC($J = 1 - 0$)	90.66356
CS($J = 2 - 1$)	97.98095
N_2H^+($J = 1 - 0$)	93.1734
C_2H($N = 1 - 0$)	87.316925[a]
^{13}CO($J = 1 - 0$)	110.20137
$C^{18}O$($J = 1 - 0$)	109.78218
^{13}CO($J = 2 - 1$)	220.398686
$C^{18}O$($J = 2 - 1$)	219.56036

Table 2. HCN has two satellite (hyperfine) lines at relative velocities of −7.1 and 4.8 km s^{-1} and relative LTE intensities of 0.2 and 0.6 respectively. These lines are generally unresolved in all but the closest extragalactic sources. HCO^+, HNC, and N_2H^+ have unresolved hyperfine structure. [a] C_2H has a total of 6 lines 87.284156, 87.316925(strongest), 87.328624 ($J = 3/2 \rightarrow 1/2$) 87.402004, 87.407165, 87.446512 ($J = 1/2 \rightarrow 1/2$).

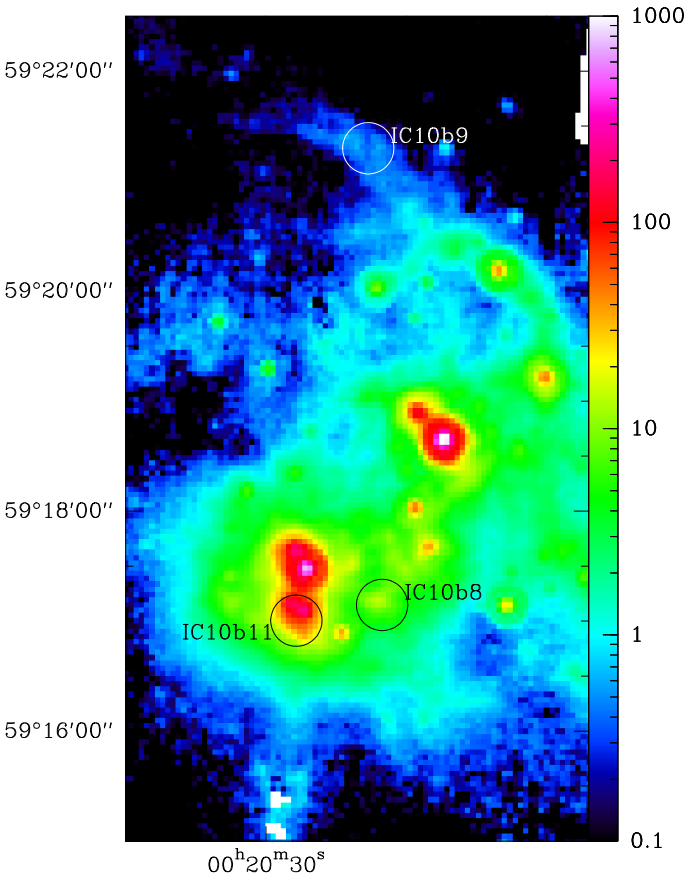

Fig. 1. Observed positions on a Spitzer 24μm map of IC10. The circle size indicates the beamwidth of the observations. Units of the 24μm emission are MJy/sr and the color scale is the same for Figures 1–3 in order to facilitate comparison.

temperature scale. The forward efficiency of the telescope is 0.95 in the 3mm band and 0.92 in the 1mm band (218–230GHz). Conversion to T_{mb} was done using main beam efficiencies of 0.59 for ^{12}CO(2–1), 0.61 for ^{13}CO(2–1) and $C^{18}O$(2–1), 0.78 for ^{12}CO(1–0) and ^{13}CO(1–0) and $C^{18}O$(1–0), 0.80 for CS(2–1), and 0.81 for HCN, HCO^+, HNC, and C_2H. All data processing was done within the GILDAS environment [2].

[2] http://www.iram.fr/IRAMFR/GILDAS/

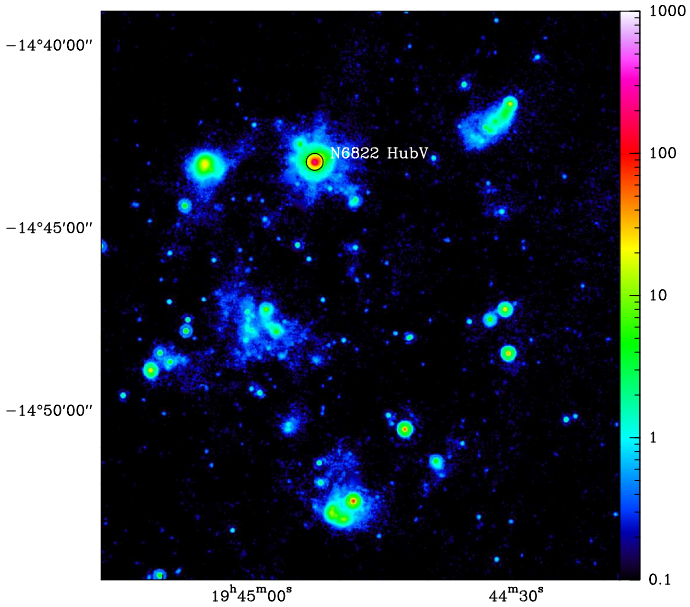

Fig. 2. Observed position on a Spitzer 24μm map of NGC 6822. The circle size indicates the beamwidth of the observations. Units of the 24μm emission are MJy/sr and the color scale is the same for Figures 1–3 in order to facilitate comparison.

2.2. Nobeyama Radio Observatory 45meter observations

The Nobeyama 45 m observations took place from May 20th to June 1st, 2015 toward the GMCs in M 33 near NGC 604. The data were taken in the position-switching mode. The TZ receiver, which is a dual polarization sideband-separating SIS receiver, was used in combination with the Fast Fourier Transform Spectrometer SAM45. To cover the ^{12}CO (1–0), ^{13}CO(1–0), $C^{18}O$(1–0), HCO^+(1–0), HCN(1–0), C_2H(1–0), HNC(1–0), SO(2,3–1,2), HC_3N (10–9) frequencies, we used three frequency settings with a bandwidth of 8 GHz (1 GHz x 8) and a frequency resolution of 244.14 kHz in the dual polarization mode. Pointing was checked by observing the IRC+30021 SiO maser emission every hour, and was shown to be accurate within 3 arcseconds. The main-beam efficiency was 38.8 - 50.0%. The system noise temperature range was 140 – 500 K. The beamsize of the NRO 45m telescope is about 19″ at 90 GHz and 15″ at 115 GHz.

We used the 4.3.1 version of the Common Astronomy Software Application (CASA) package (McMullin et al. 2007) to reduce the data obtained with the Nobeyama 45 m. The CASA package is developed for the Atacama Large Millimeter/submillimeter Array (ALMA), and is also available for reducing data obtained by a single-dish telescope such as the Nobeyama 45 m telescope. Here, we describe detailed steps of the data reduction process according to Shimajiri et al. (2015). In the first step, edge channels of each correlator band were flagged using the task *sdflag2old*, since the sensitivity of the edge channels drops. The SAM45 spectrometer of the Nobeyama 45 m telescope provides 4096 frequency channels, so that the data for the channel numbers from 1 to 300 and from 3796 to 4096 were flagged. In the second step, we determined the baseline of each spectrum using the task *sdbaselineold*. In the third step, we merged all the averaged spectra into one file using the task *sdcoadd*. In the final step, we applied the baseline correction again using the task *sdbaselineold*.

Source	I_{CO}	$I_{^{13}CO}$	$I_{C^{18}O}$	I_{HCO^+}	I_{HCN}	I_{HNC}	I_{CCH}	I_{CS}
M 33a[a]		0.64 ± .07	0.04 ± .065	0.20 ± .05	0.12 ± .05	≲ 0.06	0.09 ± .05	
M 33a[b]	15.7 ± .6	0.58 ± .10	0.21 ± .12	0.212 ± .037	0.083 ± .039	0.031 ± .036	0.117 ± .048	
M 33b[b]	15.5 ± .5	1.16 ± .12	≲ 0.11	0.806 ± .055	0.339 ± .048	0.208 ± .046	0.434 ± .068	
M 33c[b]	12.1 ± .4	0.73 ± .08	≲ 0.09	0.659 ± .046	0.496 ± .046	≲ 0.051	0.075 ± .060	
IC10b8[a]	5.54 ± .08	0.55 ± .023	≲ 0.014	0.157 ± .009	0.032 ± .010	0.025 ± .009	0.031 ± .009	≲ 0.04
IC10b9[a]	5.93 ± .08	0.46 ± .03	≲ 0.02	0.04 ± .02	≲ 0.015	≲ 0.016	≲ 0.014	0.06 ± .03
IC10b11[a]	14.9 ± .1	1.12 ± .04	0.11 ± .036	0.718 ± .023	0.245 ± .025	0.088 ± .027	0.21 ± .03	0.26 ± .05
N6822HubV[a]	2.0 ± 0.12[c]	0.16 ± .02	≲ 0.019	0.115 ± .012	0.025 ± .011	≲ 0.013	0.049 ± .012	

Table 3. New observations presented in this work. All fluxes are on the main beam temperature scale. [a] indicates observatons with the IRAM 30meter antenna and [b] with the NRO 45meter telescope. [c] taken from Gratier et al. (2010a). The other lines within the bandpasses such as SO, HC_3N, or N_2H^+, were not detected. $C^{18}O$ was not detected either but was included in this table to directly compare with ^{13}CO. Blank parts of the table indicate that the line was not observed. Limits are given as ≲ the 1σ noise level to distinguish between a tentative line (e.g. HCN in N6822HubV, 0.25 ± .011 Kkm/s) and something where there is no sign of a line (typically intensity below 1 sigma or negative).

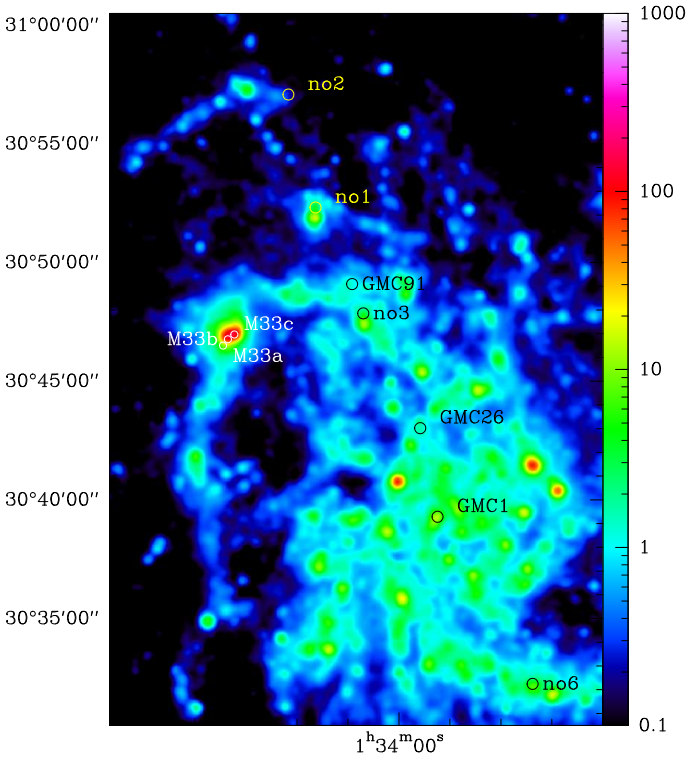

Fig. 3. Observed positions on a Spitzer 24μm map of M 33. The circle size indicates the beamwidth of the observations. Units of the 24μm emission are MJy/sr and the color scale is the same for Figures 1–3 in order to facilitate comparison. The positions and source names published in Buchbender et al. (2013) are shown as well.

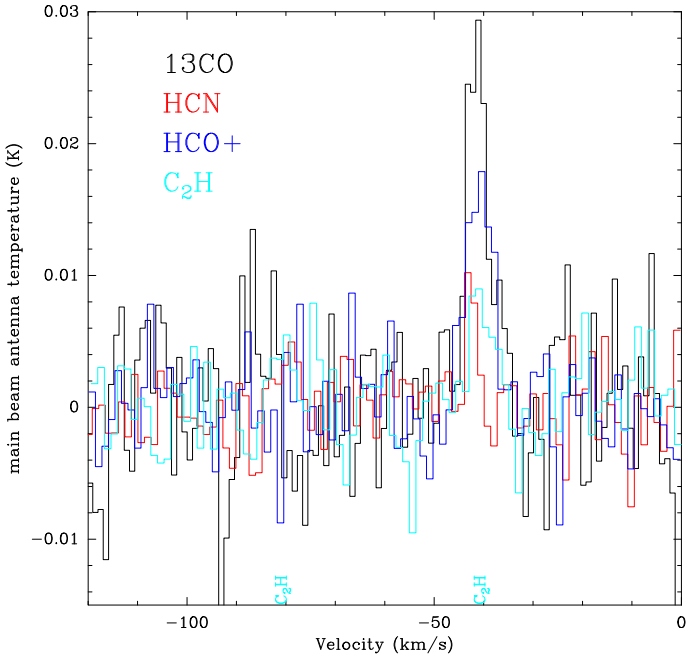

Fig. 4. ^{13}CO and dense gas tracers as observed in the Hubble V HII region in NGC 6822. Color coding is indicated in the panel.

3. Spectra and line ratios

The line intensities observed as part of the new observations are presented in Table 3. In all cases, the $C^{18}O$ lines were not detected with noise levels that place the $C^{18}O$ at typically 10% or less of the ^{13}CO line intensity. The weakness of the $C^{18}O$ relative to the more abundant isotopes is even more extreme in the Magellanic Clouds (Chin et al. 1997, 1998), where $^{13}CO/C^{18}O$ line ratios are ∼ 40, including some lower limits. In contrast, the line survey of two positions in M 51 carried out recently by Watanabe et al. (2014) showed $^{13}CO/C^{18}O$ line ratios of 4 although the $^{12}CO/^{13}CO$ line ratios are ∼ 10, similar to those of the other galaxies. The weak $C^{18}O$ emission found in these galaxies, including M 33, indicates that low ^{18}O abundance is a characteristic of subsolar metallicity environments although selective photodissociation of $C^{18}O$ likely further decreases the $C^{18}O$ emission (Shimajiri et al. 2014).

Figures 4 – 6 present the spectra of the main (detected) lines of interest – ^{13}CO(1–0), HCN(1–0), HCO^+(1–0), C_2H, and ^{12}CO(1–0). It is immediately apparent that the HCN lines are weak relative to HCO^+. This was already seen in the observations of the Magellanic Clouds presented by Chin et al. (1997) and Chin et al. (1998). It was also noted for M 33 by Buchbender et al. (2013), as compared to M 31 (Brouillet et al. 2005) where the HCN and HCO^+ intensities are similar. Watanabe et al. (2014) find stronger HCN than HCO^+ emission near the nucleus of M 51. Bigiel et al. (2016) found generally stronger HCN emission compared to HCO^+ in the inner disk of M 51. The metallicity of M 51 is solar or somewhat higher and decreases with distance from the galactic center (Bresolin et al. 2004). Several clouds in the outskirts of M 51 were observed by Chen et al. (2016) who found similar HCN and HCO^+ fluxes (slightly stronger HCO^+). All these works found that the HNC

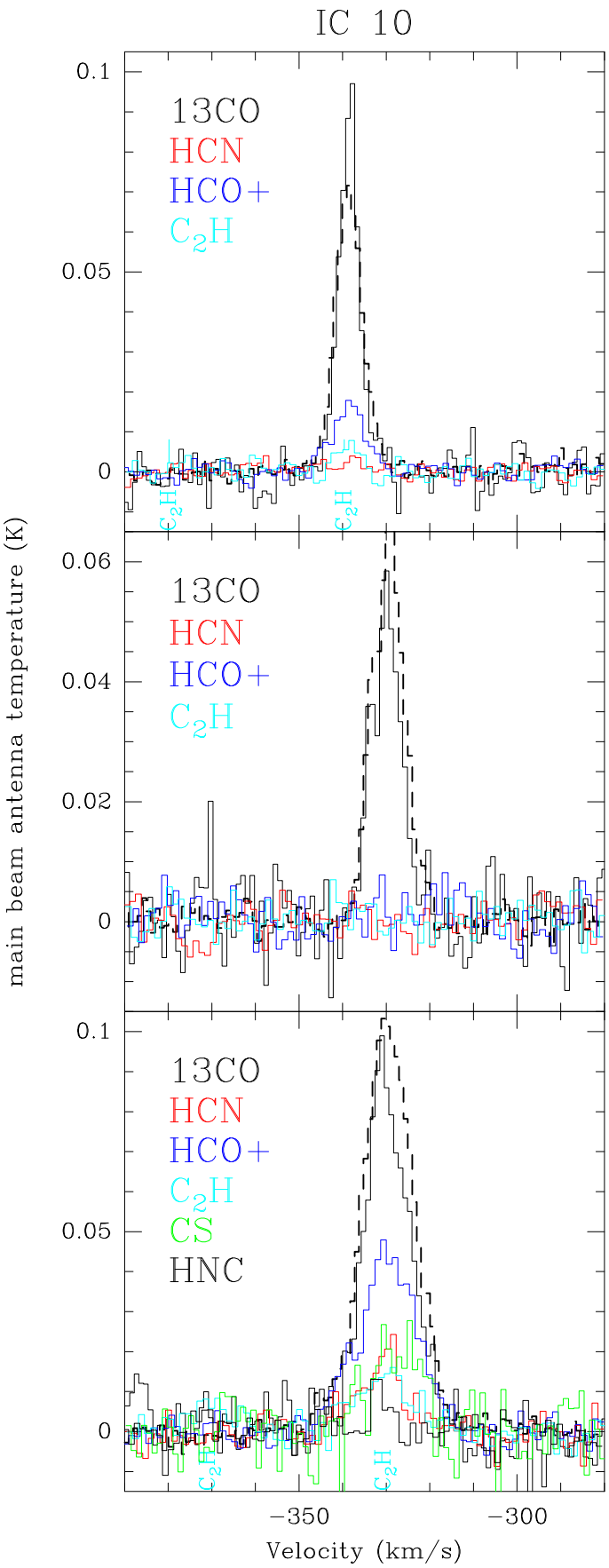

Fig. 5. ^{13}CO, ^{12}CO and dense gas tracers as observed in the b8, b9, and b11 regions in IC 10. Color coding is indicated in the panel. Note that additional lines were detected in IC 10 b11. The ^{12}CO line scale (dashed) is divided by 10.

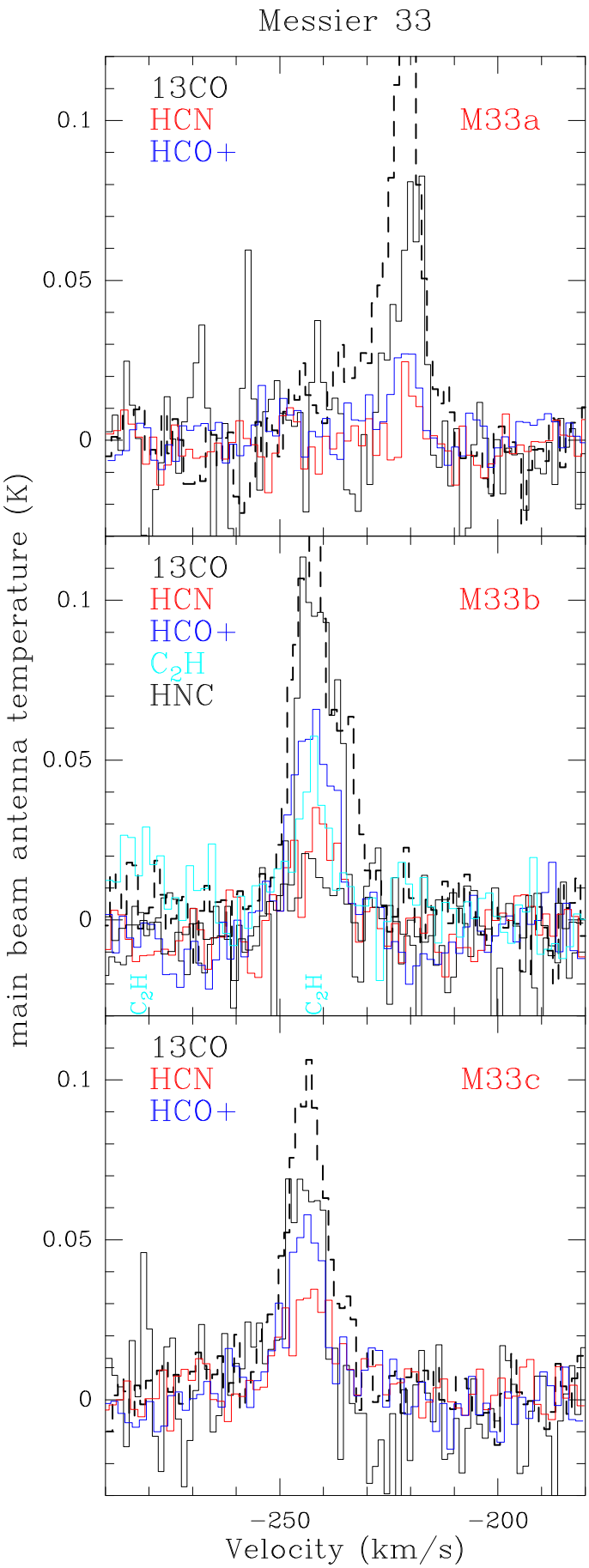

Fig. 6. ^{13}CO, ^{12}CO and dense gas tracers as observed in the M 33a, M 33b, and M 33c regions in M 33, all near the giant HII region NGC 604. Color coding is indicated in the panel. Note that additional lines were detected in M 33b. The ^{12}CO line scale (dashed) is divided by 10.

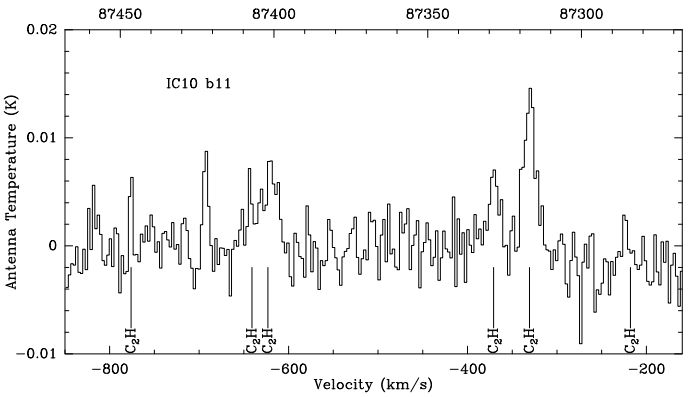

Fig. 7. C_2H spectrum observed in source b11 in the galaxy IC10. Upper scale gives the rest frequency in MHz. The 6 transitions are marked. The flux ratios are compatible with LTE.

emission from M 51 was 20–50% of the HCN strength. This HNC/HCN ratio is consistent with our data and those presented by Chin et al. (1997) and Chin et al. (1998) but higher than found by Buchbender et al. (2013) in their stacked spectrum.

The spectra presented by Watanabe et al. (2014) can be straightforwardly compared with our own. They detect the N_2H^+ and HNCO lines at a level stronger than the C_2H lines and 5–10% of the $^{13}CO(1–0)$ line strength. These lines are not detected in the low-metallicity systems. The CN lines are strong in M 51, 10–15% of the $^{13}CO(1–0)$ line strength. The $^{13}CO/^{12}CO$ line ratio is nearly constant among the sources, almost irrespective of metallicity, so we choose these lines as a reference to compare relative line strengths. Neither we nor Buchbender et al. (2013) detect CN, even in stacked spectra. However, since we observed CN simultaneously with $^{12}CO(1–0)$, a strong line, the limits are of order 10% of the $^{13}CO(1–0)$ intensity, and less constraining in some cases. The limits to the CN emission show, for the Buchbender et al. (2013) sources and IC10 (the other upper limits in our data are not constraining), that it is weaker than HCN and C_2H but consistent with the observations of the LMC by Chin et al. (1997).

In addition to $C^{18}O$, the weak and/or non-detected lines are all of Nitrogen bearing molecules. Not only is the CO luminosity per H_2 mass low in subsolar metallicity systems but the Nitrogen-bearing molecules are weak relative to CO. The C_2H lines on the other hand are not weak relative to CO. Figure 7 shows the clearest of our C_2H spectra, including most or all of the 6 components. While the S/N ratio is low for the weaker components, the fluxes are consistent with the ratios expected at Local Thermodynamic Equilibrium (LTE).

Tercero et al. (2010) observed Orion KL with the IRAM 30meter telescope. As can be seen from their Fig. 2, the HCN and $H^{13}CN$ lines are much stronger than the HCO^+ and $H^{13}CO^+$ lines respectively. These lines are just an example as generally, in this gas exposed an extremely high radiation field, the line ratios are different both from M 51 and lower metallicity sources. Nishimura et al. (2016) observed position IC10b11 with the NRO 45m and obtain similar detections and non-detections.

4. Source of the variations in line ratios

HCN and HCO^+ have similar dipole moments and are both linear molecules, with a substitution of O^+ for N in the latter. It is thus reasonable to expect a link between the N/O abundance ratio and the abundance ratio of the two molecules.

For the range in metallicities of our sources, the N/O abundance ratio is roughly proportional to the Oxygen abundance (O/H) although the N/O ratio appears roughly constant for lower metallicities (see Figures 3–4 and 5 in Pilyugin et al. 2003; van Zee & Haynes 2006, respectively). This is attributed to a change in the origin of Nitrogen from primary at low metallicity to secondary at higher metallicity.

Figure 8 shows the variation of the HCN/HCO^+ line intensity ratio. Both of these lines are optically thick in dense regions of the Galaxy but at these metallicities and scales (10-100 pc), the lines are expected to be optically thin, with the possible exception of M 31. In Fig. 8, each galaxy has been assumed to have the same metallicity for all positions. M 33 and M 31 only have weak metallicity gradients (Magrini et al. 2009; Sanders et al. 2012) and the others have no known gradient although there may be metallicity inhomogeneities. An increase in the HCN/HCO^+ line intensity ratio from roughly 1/4 at a metallicity of 0.3 solar to about 0.9 in M 31 follows this trend in N/O abundance. At these scales, we have no reason to invoke other sources than the N/O abundance ratio to explain the observed trend in the HCN/HCO^+ line intensity ratio with metallicity. The N/O abundance ratio was also proposed by Anderson et al. (2014) as a possible explanation of the low HCN/HCO^+ ratio in the LMC.

5. Link with star formation

Figure 9 shows the link between the dense gas fraction, as traced by the intensity ratios of HCN and HCO^+ to CO, and the SFR as traced by the 24μm emission. When the 24μm emission is strong, both the HCN/CO and HCO^+/CO ratios are high and the relation appears monotonic. However, the HCO^+/CO ratio shows less scatter between the galaxies (M 33 and IC10) than the HCN/CO line ratio, presumably due to the lesser effect of metallicity variations which cause the HCN/CO ratios of IC10 to be lower than in M 33. Therefore, at the 100pc scale, it appears that HCO^+ may be the preferred tracer of dense gas in low-metallicity objects.

Buchbender (2014) observed HCN, HCO^+, and CO in cloud no3 in M 33 at a resolution of about 20pc. From his figure 11.3, clear differences at this scale are seen between the distribution of the two lines. His figure 11.5 shows a comparison of the HCN and HCO^+ maps with various star formation tracers.

The observations presented here are at a scale of 100pc (range of 70–140pc), intermediate between the subpc-scale Galactic data and the typically kpc or whole-galaxy extragalactic measurements. Figure 10 shows how the HCN and HCO^+ luminosities compare with Galactic and extragalactic observations at various scales. Points above the line can be considered to have weak line emission and those below to have strong line emission. The trend is basically a linear relation between the emission of the dense gas tracers and IR luminosity, presumably reflecting a proportionality between the mass of dense gas and the star formation rate. However, and this is why we have chosen to separate galactic centers and inner disks from outer regions, the physical conditions in large galaxies are such that stellar surface densities and molecular fractions are systematically higher in the inner disk as compared to external regions (Chen et al. 2015; Usero et al. 2015). Furthermore, spirals show radial metallicity gradients.

Looking at the data points above and below the line showing HCN-IR proportionality, it is immediately clear that HCN is relatively stronger in the inner regions (Chen et al. 2015; Krips et al. 2008) and weaker in low-metallicity galaxies (points from Chin et al. 1997, 1998; Buchbender et al. 2013, and this

work). Turning to the HCO^+ emission in the lower panel, the linear relation appears to have less systematic scatter in that the low-Z points are not off the global fit and inner disk points are closer to it. However, fewer extragalactic HCO^+ data are available. Figure 11 expands the vertical scale by plotting the ratio of the IR-to-HCN (or HCO^+) luminosity as a function of the IR luminosity. Here it becomes apparent that at the small scales observed by Ma et al. (2013) and Wu et al. (2005), the IR emission increases more rapidly than the HCN or HCO^+. This could be due to either an increase in the line optical depth, causing saturation for the more massive clumps, or, as suggested by Wu et al. (2010), that the IR luminosity of low-mass star forming regions decreases more quickly due to an incomplete sampling of the IMF such that few (if any) massive stars are present.

One would expect high redshift objects to have generally subsolar metallicities and, due to their necessarily young ages, low N/O abundance ratios (much of the Nitrogen production occurs after a substantial time delay). The observations of high-redshift objects, necessarily very bright, by Gao et al. (2007) seem to go in this direction as the HCN emission per unit IR luminosity is weak (or equivalently the IR emission is strong). The HCN/IR ratio is about a factor of 2 weaker compared to that established in local galaxies, yet this value is similar to what we found here in nearby low-Z galaxy systems. Nevertheless, the HCN/CO ratios of the low-Z systems and high-redshift AGNs/ULIRGs are at the two extreme ends, the smallest HCN/CO values are found in low-Z whereas the highest are in high redshift AGNs/ULIRGs, similar to that of local ULIRGs despite their higher HCN/IR ratio. It is still unclear whether low N/O abundance ratios could explain all the differences. Therefore, the low HCN/IR ratio at high redshift might suggest a higher star formation rate per unit dense molecular gas in high-redshift AGNs/ULIRGs, although not necessarily so in nearby low-Z systems, compared to those of local normal star-forming galaxies. HCO^+ measurements would greatly help to determine the appropriate interpretation.

6. Summary and Conclusions

The low-metallicity Local Group galaxies NGC 6822, IC 10, and M 33 have been observed in a number of molecular lines, including the dense gas tracers HCN(1–0) and HCO^+(1–0), at a scale of 70–140 pc. In addition to ^{12,13}CO, HCO^+, HCN, HNC, C_2H, and CS(2–1) have been detected in one or more objects.

The HCN and HNC lines are weak with respect to the IR or ^{12,13}CO emission but the HCO^+ follows the trends observed in solar metallicity galaxies. $C^{18}O$, N_2H^+, CN, and HNCO were not detected although in M 51 (Watanabe et al. 2014) these lines are stronger than C_2H, which was well detected. N/O varies as O/H at the metallicities explored here. An accordingly low Nitrogen abundance could explain the weakness of the Nitrogen-bearing species in our observations and more generally in the observations of low metallicity galaxies.

The SFR, as traced by the 24 um emission, increases with the dense gas fraction, as traced by the HCN/CO or HCO^+/CO line ratios.

The low–Z points fall below (i.e. less HCN) the linear HCN–IR Galactic-extragalactic luminosity correlation but right on the HCO^+–IR correlation. When measuring the dense gas mass of low metallicity objects, HCO^+ may be a more robust tracer than HCN.

Acknowledgements. JB would like to thank Laura Magrini for very useful discussions about abundances and abundance gradients in galaxies. We would also like to thank Belen Tercero for the the data enabling us to calculate the line ratios of interest in Orion KL. The authors would like to acknowledge support from the French Agence Nationale de Recherche (ANR) grant ANR-11-BS56-010 for the STARFICH project (www.obs.u-bordeaux1.fr/webformationetoiles/StarFichE) and the European Research Council under the European Union's Seventh Framework Programme (ERC Advanced Grant Agreement no. 291294 – 'ORISTARS'). YG acknowledges support from the National Natural Science Foundation of China (NSFC grants 11390373 and 11420101002), the Strategic Priority Research Program "The Emergence of Cosmological Structures" (grant XDB09000000) and Key Research Program of Frontier Sciences of the Chinese Academy of Sciences.

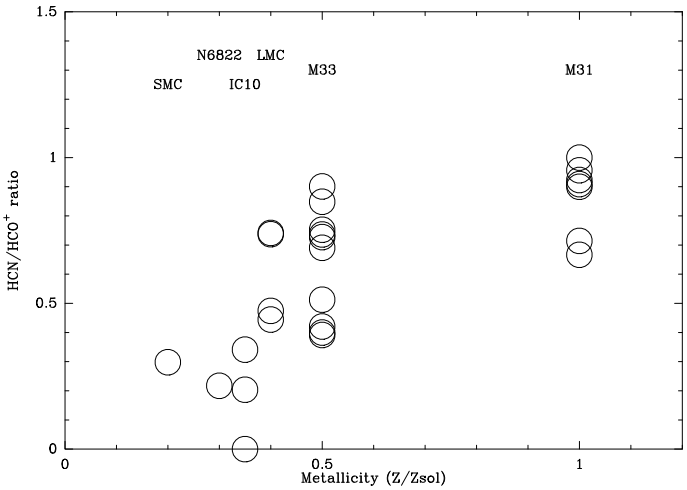

Fig. 8. Variation of the HCN/HCO^+ ratio with metallicity. References are Brouillet et al. (2005); Chin et al. (1997, 1998) for M 31 and the Magellanic Clouds, Buchbender et al. (2013) and the present work for M 33, and this work for IC 10 and NGC 6822. Typical uncertainties for individual points are 0.2 dex for the metallicity and 0.3 in the HCN/HCO^+ ratio.

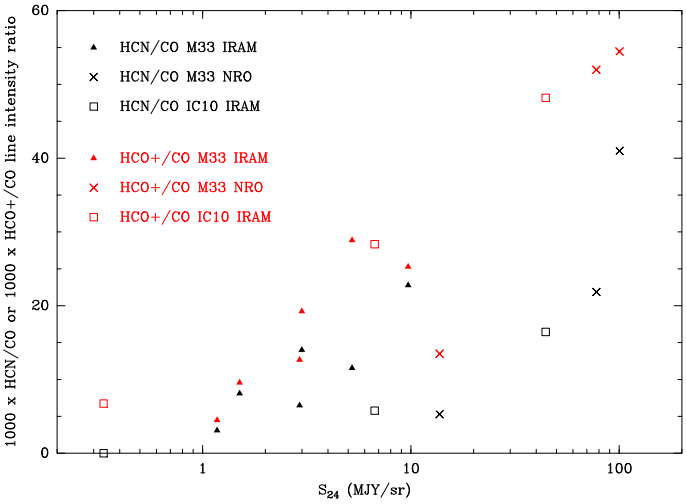

Fig. 9. Link between dense gas fraction and star formation rate. The HCN/CO and HCO^+/CO ratios are used to trace the fraction of dense molecular gas and the 24μm intensity is used as a proxy for the SFR. HCN/CO is in black and HCO^+/CO is in red. Observations are from Buchbender et al. (2013) and the present work. Typical uncertainties are 20% for HCO^+/CO and 25% for the HCN/CO ratio.

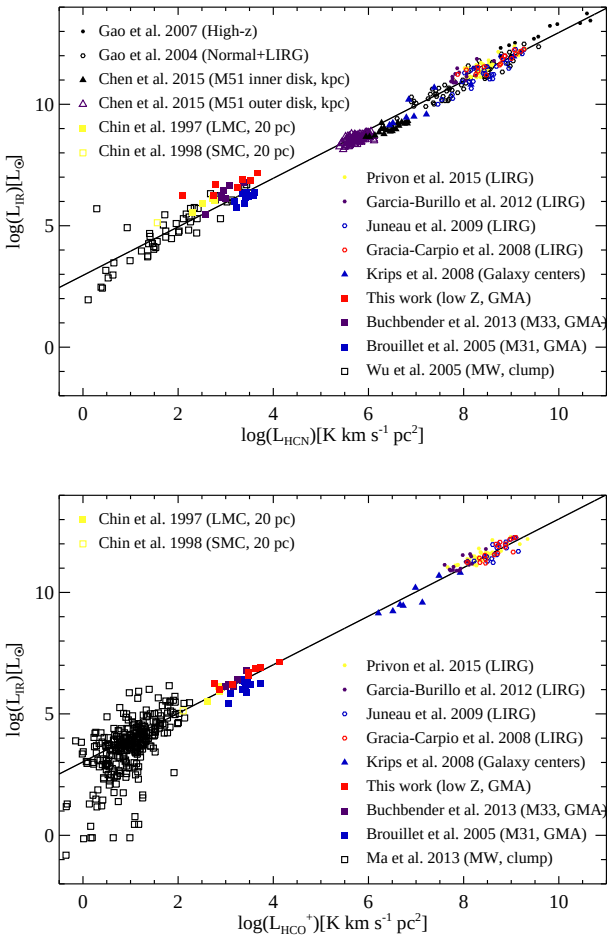
Gao et al. 2007 (High-z)
Gao et al. 2004 (Normal+LIRG)
Chen et al. 2015 (M51 inner disk, kpc)
Chen et al. 2015 (M51 outer disk, kpc)
Chin et al. 1997 (LMC, 20 pc)
Chin et al. 1998 (SMC, 20 pc)
Privon et al. 2015 (LIRG)
Garcia-Burillo et al. 2012 (LIRG)
Juneau et al. 2009 (LIRG)
Gracia-Carpio et al. 2008 (LIRG)
Krips et al. 2008 (Galaxy centers)
This work (low Z, GMA)
Buchbender et al. 2013 (M33, GMA)
Brouillet et al. 2005 (M31, GMA)
Wu et al. 2005 (MW, clump)
log(L_IR)[L_⊙]
log(L_HCN)[K km s^-1 pc^2]
Chin et al. 1997 (LMC, 20 pc)
Chin et al. 1998 (SMC, 20 pc)
Privon et al. 2015 (LIRG)
Garcia-Burillo et al. 2012 (LIRG)
Juneau et al. 2009 (LIRG)
Gracia-Carpio et al. 2008 (LIRG)
Krips et al. 2008 (Galaxy centers)
This work (low Z, GMA)
Buchbender et al. 2013 (M33, GMA)
Brouillet et al. 2005 (M31, GMA)
Ma et al. 2013 (MW, clump)
log(L_IR)[L_⊙]
log(L_HCO+)[K km s^-1 pc^2]

Fig. 10. Link between IR luminosity and HCN (upper panel) and HCO^+ (lower panel) luminosity. The lines show a linear relation between the two quantities. The fits are $log(L_{IR}) = 2.95424 + log(L_{HCN})$ and $log(L_{IR}) = 3.04258 + log(L_{HCO^+})$ and are from respectively Gao & Solomon (2004b) and Graciá-Carpio et al. (2008). The symbols indicate the reference and the scale of the observation.

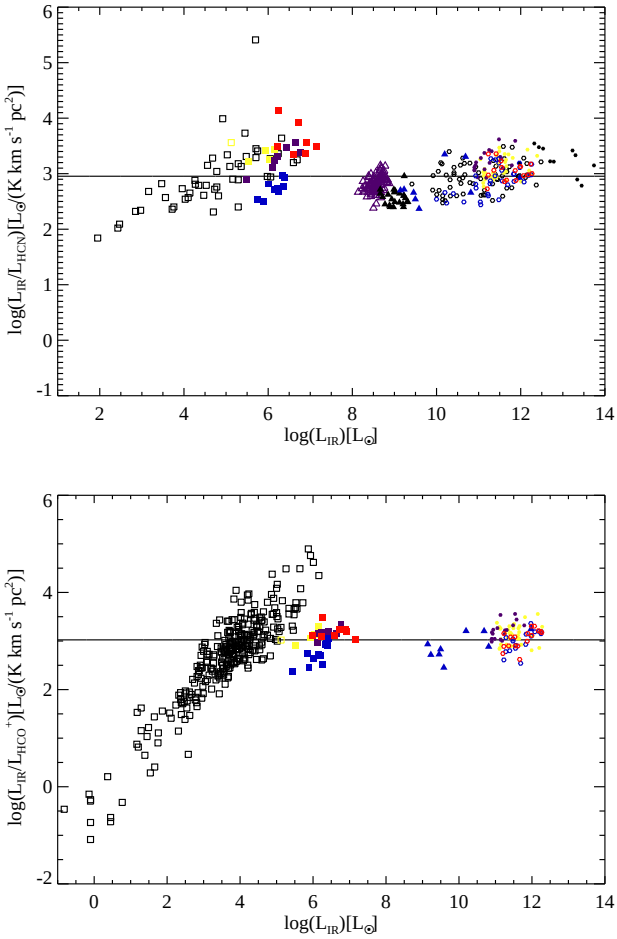

Fig. 11. Ratio between IR and HCN (upper panel) and HCO^+ (upper panel) luminosities as a function of IR luminosity. The goal here is to see finer structure than in the previous figure as the vertical scale has been greatly expanded. References are as given in Fig. 10.

References

Anderson, C. N., Meier, D. S., Ott, J., et al. 2014, ApJ, 793, 37
André, P., Di Francesco, J., Ward-Thompson, D., et al. 2014, Protostars and Planets VI, 27
André, P., Men'shchikov, A., Bontemps, S., et al. 2010, A&A, 518, L102
Baan, W. A., Henkel, C., Loenen, A. F., Baudry, A., & Wiklind, T. 2008, A&A, 477, 747
Bigiel, F., Leroy, A. K., Jiménez-Donaire, M. J., et al. 2016, ApJL, 822, L26
Boquien, M., Calzetti, D., Combes, F., et al. 2011, AJ, 142, 111
Bresolin, F., Garnett, D. R., & Kennicutt, Jr., R. C. 2004, ApJ, 615, 228
Brouillet, N., Muller, S., Herpin, F., Braine, J., & Jacq, T. 2005, A&A, 429, 153
Buchbender, C. 2014, PhD thesis, Universidad de Granada, http://hdl.handle.net/10481/31707
Buchbender, C., Kramer, C., Gonzalez-Garcia, M., et al. 2013, A&A, 549, A17
Calzetti, D., Wu, S.-Y., Hong, S., et al. 2010, ApJ, 714, 1256
Carter, M., Lazareff, B., Maier, D., et al. 2012, A&A, 538, A89
Chen, H., Braine, J., Gao, Y., Koda, J., & Gu, Q. 2016, ApJ, submitted
Chen, H., Gao, Y., Braine, J., & Gu, Q. 2015, ApJ, 810, 140
Chin, Y.-N., Henkel, C., Millar, T. J., Whiteoak, J. B., & Marx-Zimmer, M. 1998, A&A, 330, 901
Chin, Y.-N., Henkel, C., Whiteoak, J. B., et al. 1997, A&A, 317, 548
Druard, C., Braine, J., Schuster, K. F., et al. 2014, A&A, 567, A118
Galametz, M., Kennicutt, R. C., Calzetti, D., et al. 2013, MNRAS, 431, 1956
Galleti, S., Bellazzini, M., & Ferraro, F. R. 2004, A&A, 423, 925
Gao, Y., Carilli, C. L., Solomon, P. M., & Vanden Bout, P. A. 2007, ApJL, 660, L93
Gao, Y. & Solomon, P. M. 2004a, ApJS, 152, 63
Gao, Y. & Solomon, P. M. 2004b, ApJ, 606, 271
García-Burillo, S., Usero, A., Alonso-Herrero, A., et al. 2012, A&A, 539, A8
Graciá-Carpio, J., García-Burillo, S., Planesas, P., Fuente, A., & Usero, A. 2008, A&A, 479, 703
Gratier, P., Braine, J., Rodriguez-Fernandez, N. J., et al. 2010a, A&A, 512, 68
Gratier, P., Braine, J., Rodriguez-Fernandez, N. J., et al. 2010b, A&A, 522, 3
Heiderman, A., Evans, II, N. J., Allen, L. E., Huard, T., & Heyer, M. 2010, ApJ, 723, 1019
Hirota, T., Yamamoto, S., Mikami, H., & Ohishi, M. 1998, ApJ, 503, 717
Hunter, D. A. 2001, ApJ, 559, 225
Juneau, S., Narayanan, D. T., Moustakas, J., et al. 2009, ApJ, 707, 1217
Kepley, A. A., Leroy, A. K., Frayer, D., et al. 2014, ApJL, 780, L13
Krips, M., Neri, R., García-Burillo, S., et al. 2008, ApJ, 677, 262
Kuno, N., Nakai, N., Handa, T., & Sofue, Y. 1995, PASJ, 47, 745
Lada, C. J., Forbrich, J., Lombardi, M., & Alves, J. F. 2012, ApJ, 745, 190
Lada, C. J., Lombardi, M., & Alves, J. F. 2010, ApJ, 724, 687
Leroy, A., Bolatto, A., Walter, F., & Blitz, L. 2006, ApJ, 643, 825
Liu, F. & Gao, Y. 2010, ApJ, 713, 524
López-Sepulcre, A., Cesaroni, R., & Walmsley, C. M. 2010, A&A, 517, A66
Ma, B., Tan, J. C., & Barnes, P. J. 2013, ApJ, 779, 79
Magrini, L. & Gonçalves, D. R. 2009, MNRAS, 398, 280
Magrini, L., Stanghellini, L., & Villaver, E. 2009, ApJ, 696, 729
Mateo, M. L. 1998, ARA&A, 36, 435
McMullin, J. P., Waters, B., Schiebel, D., Young, W., & Golap, K. 2007, in Astronomical Society of the Pacific Conference Series, Vol. 376, Astronomical Data Analysis Software and Systems XVI, ed. R. A. Shaw,

F. Hill, & D. J. Bell, 127
Meier, D. S. & Turner, J. L. 2005, ApJ, 618, 259
Nishimura, Y., Shimonishi, T., Watanabe, Y., et al. 2016, ApJ, 829, 94
Pilyugin, L. S., Thuan, T. X., & Vílchez, J. M. 2003, A&A, 397, 487
Privon, G. C., Herrero-Illana, R., Evans, A. S., et al. 2015, ApJ, 814, 39
Sanders, N. E., Caldwell, N., McDowell, J., & Harding, P. 2012, ApJ, 758, 133
Shimajiri, Y., Kitamura, Y., Saito, M., et al. 2014, A&A, 564, A68
Shimajiri, Y., Sakai, T., Kitamura, Y., et al. 2015, ApJS, 221, 31
Skillman, E. D., Kennicutt, R. C., & Hodge, P. W. 1989, ApJ, 347, 875
Tennekes, P. P., Harju, J., Juvela, M., & Tóth, L. V. 2006, A&A, 456, 1037
Tercero, B., Cernicharo, J., Pardo, J. R., & Goicoechea, J. R. 2010, A&A, 517, A96
Usero, A., Leroy, A. K., Walter, F., et al. 2015, AJ, 150, 115
van Zee, L. & Haynes, M. P. 2006, ApJ, 636, 214
Watanabe, Y., Sakai, N., Sorai, K., & Yamamoto, S. 2014, ApJ, 788, 4
Wu, J., Evans, II, N. J., Gao, Y., et al. 2005, ApJ, 635, L173
Wu, J., Evans, II, N. J., Shirley, Y. L., & Knez, C. 2010, ApJS, 188, 313